Design of Few-Mode Fibers with *M*-modes and Low Differential Mode Delay

Filipe Ferreira, *Student Member, IEEE,* Daniel Fonseca, and Henrique Silva, *Member, IEEE*

***Abstract*—In this paper, we investigate the design of few-mode fibers (FMFs) guiding 2 to 12 linearly polarized (LP) modes with low differential mode delay (DMD) over the C-band, suitable for long-haul transmission. Two different types of refractive index profile have been considered: a graded-core with a cladding trench (GCCT) profile and a multi-step-index (MSI) profile. The profiles parameters are optimized in order to achieve: the lowest possible DMD and macro-bend losses (MBL) lower than the ITU-T standard recommendation. The optimization results show that the MSI profiles present lower DMD than the minimum achieved with a GCCT profile. Moreover, it is shown that the optimum DMD and the MBL scale with the number of modes for both profiles. The optimum DMD obtained for 12 LP modes is lower than 3 ps/km using a GCCT profile and lower than 2.5 ps/km using a MSI profile. The optimization results reveal that the most preponderant parameter of the GCCT profile is the refractive index relative difference at the core center, Δn_{co}. Reducing Δn_{co}, the DMD is reduced at the expense of increasing the MBL. Regarding the MSI profiles, it is shown that 64 steps are required to obtain a DMD improvement considering 12 LP modes. Finally, the impact of the fabrication margins on the optimum DMD is analyzed. The probability of having a manufactured FMF with 12 LP modes and DMD lower than 12 ps/km is approximately 68 % using a GCCT profile and 16 % using a MSI profile.**

***Index Terms*—Few-Mode Fibers, Differential Mode Delay, Refractive Index Profile.**

I. Introduction

THE ever growing demand for higher data rate is rapidly exhausting the capacity available for single-mode fibers (SMFs). During the last years, only a marginal increase in the maximum bit rate distance product using SMFs was observed [1], since the nonlinear Shannon limit is being reached [2]. Moreover, it has been demonstrated that even if significant reduction of the fiber attenuation or of the fiber nonlinear coefficient of standard SMFs (SSMFs) are achieved, the capacity increase per fiber is limited [3].

Mode-division multiplexing (MDM) over few-mode fibers (FMFs) is emerging as an attractive solution for the required capacity increase with potential cost, space, and energy savings [3]-[4]. However, FMFs require the usage of multiple-input multiple-output (MIMO) equalization to compensate for the combined effect of differential mode delay (DMD) and modal crosstalk (XT), which originates a channel impulse response (CIR) spread over time [5]. Therefore, the additional processing complexity partially erodes the benefit of deploying FMFs. It has been shown in [6] that, considering similar levels of complexity for nonlinearity mitigation in a SSMF, only FMF systems with 4 or more LP modes offer an actual capacity increase. One of the approaches proposed to reduce the equalizer complexity is the minimization of XT along the transmission system so that each mode can be detected individually without MIMO processing. However, experimental interfaces/couplers with such property present high loss [7]. We follow another approach in this paper, the reduction of DMD, and investigate techniques to design FMFs with low DMD over the C-band from 2 to 12 LP modes.

In the literature, two different schemes have been proposed to limit the accumulation of DMD in FMFs with *x* modes (*x*M): the usage of inherently low DMD FMFs (ILD-FMFs) [8]-[11], and the usage of DMD compensated FMFs (DC-FMFs) (FMFs with positive DMD followed by FMFs with negative DMD) [12]-[17]. The main target in this paper is a DMD lower than 12 ps/km over the C-band, since this is the DMD required for 2000 km of MDM transmission at 100 Gb/s using an overhead of up to 10% [5]. Note that the DMD should be lower than 12 ps/km over the C-band, in order to allow the transmission of wavelength-division-multiplexing signals. In [17] a 4M-DC-FMF with 59 km and a differential group delay of 350 ps over the C-band (the equivalent DMD is 5.9 ps/km) allowing long-haul transmission was presented. However, such tightly DMD compensated span required 4 FMFs with different DMDs. Moreover, increasing *x*M an even higher number of FMFs with different DMDs will be required, imposing difficulties in the field deployment compared to ILD-FMFs. Therefore, in this paper we investigate only ILD-FMFs. The ILD-FMFs considered have mainly two types of refractive index profile: graded-core with cladding trench (GCCT) [8]-[9], [11]-[15], and multi-step-index (MSI) [10],

Manuscript received Month 00, 2013; revised Month 00, 2013; accepted Month 00, 2013. Date of publication Month 00, 2013. Manuscript received Month 00, 2013. This work was supported in part by Coriant Portugal, Fundação para a Ciência e Tecnologia under Grant SFRH/BDE/51094/2010 and in part by European Communities 7th Framework Programme under Grant Agreement 258033.

F. Ferreira is with Coriant Portugal, 2720-093 Amadora, Portugal, and also with Instituto de Telecomunicações, Universidade de Coimbra, 3030-290 Coimbra, Portugal (e-mail: filipe.ferreira@coriant.com).

D. Fonseca is with Coriant Portugal, 2720-093 Amadora, Portugal, and also with Instituto de Telecomunicações, 1049-001 Lisboa, Portugal (e-mail: daniel.fonseca@coriant.com).

H. Silva is with Instituto de Telecomunicações, Universidade de Coimbra, 3030-290 Coimbra, Portugal (e-mail: hjas@co.it.pt).

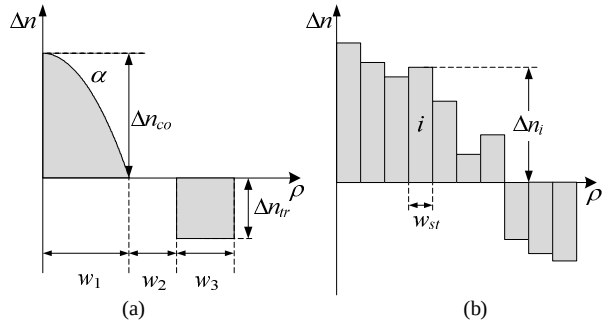

Fig. 1. (a) GCCT profile. (b) MSI profile with constant w_{st}.

[16]. The experimental and simulation based reports of 2M-ILD-FMFs presented in the literature have shown a DMD over the C-band lower than 6 ps/km along 10 km [9] and lower than 25 ps/km along 50 km [11]. In [18] we demonstrated the possibility of obtaining a GCCT profile for a 2M-ILD-FMF with negligible DMD over the C-band. However, for 4M-ILD-FMFs, several DMD values times higher than 12 ps/km have been reported: [15] presented a DMD lower than 135 ps/km along 7 km over C+L band using a GCCT profile, and [10] presented a DMD lower than 20 ps/km over only 0.4 nm using a MSI profile with 18 steps (simulation result). In [19] we optimized a GCCT profile for 4M and 6M, obtaining DMD values of 5 and 10 ps/km, respectively, over the C-band. Therefore, further improvement on the design of ILD-FMFs is required, in order to achieve cost-effective long-haul transmission systems.

In this work, the optimization of a GCCT profile and of a MSI profile is performed for 2M to 12M, with the objective of obtaining a DMD lower than the 12 ps/km over the C-band requirement. Although the GCCT profile designs have presented lower DMD over a wider wavelength range, the MSI profile is also considered in order to evaluate alternative profiles. The optimization of the GCCT profile proposed in this paper extends the work that we presented in [18] and [19]. As the optimized DMD grows significantly with *x*M [19], we proposed to optimize the refractive index relative difference at the core center, Δn_{co}, which was fixed in [18]-[19]. However, as Δn_{co} has a direct impact on the macro-bend losses (MBL) [20], we take into account such impact on the optimization function. Finally, the impact of fabrication margins on the DMD of the optimum profiles is analyzed, since high sensitivity of FMFs to such margins has already been identified [9] and [18]. The paper is organized as follows. Section II describes the profiles considered and provides an analysis of the impact of their parameters on DMD and MBL. Section III presents the optimization function algorithms. Section IV presents the optimization results, whereas Section V presents the tolerance to the fabrication margins of the optimum designs. Section VI summarizes the main conclusions of this paper.

II. Fiber Profile Description and Analysis

In this section the GCCT and MSI profiles are described using the refractive index relative difference (Δn). Δn is a function of the radial coordinate ρ, and is given by: $\Delta n(\rho) = [n(\rho) - n_{cl}]/n(\rho)$, where $n(\rho)$ is the refractive index at ρ and n_{cl} is the cladding refractive index. For both profiles, the guided modes (LP$\mu\nu$) and their characteristics are calculated solving the Maxwell equations numerically using the method described in [21]. The LP$\mu\nu$ mode characteristics calculated are the effective index $\bar{n}^{LP\mu\nu}$, the effective group index $\bar{n}_g^{LP\mu\nu}$, the DMD and the MBL. The DMD of the LP$\mu\nu$ mode is measured relatively to the LP01 mode and is given by $DMD_{LP\mu\nu}(\lambda) = [\bar{n}_g^{LP\mu\nu}(\lambda) - \bar{n}_g^{LP01}(\lambda)] / c$, where λ is the wavelength and c is the light velocity in vacuum. The MBL are calculated according to [20]. The dispersion properties of the doped silica have been modeled using the Sellmeier coefficients provided in [22].

The GCCT profile is presented in Fig. 1 (a) and analytically described by:

$$n(\rho) = \begin{cases} n(0)\left[1-\Delta n_{co}\left(\rho/w_1\right)^{\alpha}\right], & |\rho| < w_1 \\ n_{cl}, & w_1 \le |\rho| < w_1 + w_2 \\ n_{cl}/\left(1-\Delta n_{tr}\right), & w_1 + w_2 \le |\rho| < w_1 + w_2 + w_3 \\ n_{cl}, & |\rho| \ge w_1 + w_2 + w_3 \end{cases} \quad (1)$$

where w_1 is the core radius, w_2 is the radial distance between the end of the core and the beginning of the trench, w_3 is the trench width, $\Delta n_{co} = \Delta n(0)$, and Δn_{tr} is Δn at the trench. When designing a graded core fiber with a given *x*M, one must first choose the normalized frequency (V) value. V is given by:

$$V = \frac{2\pi w_1}{\lambda} \cdot \left[n_{co}^2 - n_{cl}^2\right]^{1/2} \quad (2)$$

where $n_{co} = n(0)$. For each *x*M fiber, we choose the highest possible V value that guarantees the guidance of the first *x*-modes while cutting off the next higher-order modes, as in [23], considering a GCCT profile with $\alpha = 2.3$ and $\Delta n_{tr} = 0$. As a result, for 2M, 4M, 6M, 9M and 12M, the V values are chosen to be 5.10 [18], 7.25 [19], 9.00 [19], 11.15 and 12.95, respectively. As a consequence, the *x*-modes have the highest possible $\bar{n}^{LP\mu\nu}$ values and are thus more strongly guided. The w_1 for each *x*M fiber is obtained using (2) and considering the lowest λ of the C-band (1530 nm). Along this paper, references to a Δn_{co} change imply a w_1 change such that V remains constant.

The impact of α and Δn_{tr} on the DMD of a GCCT profile was explained in [18] for a 2M-FMF: α allows controlling the DMD average and Δn_{tr} allows controlling the DMD slope. In the following, the impact of Δn_{co} on the DMD of a GCCT profile is explained, considering a 2M-FMF with $\alpha = 2$ and $\Delta n_{tr} = 0$. Fig. 2 shows the DMD as a function of λ, for different Δn_{co} values (very low Δn_{co} values are considered in order to increase its impact). From Fig. 2 one can conclude that the DMD decreases with Δn_{co}, over a wide wavelength range. Further reducing Δn_{co}, negligible levels of DMD are obtained since, for an infinitesimal Δn_{co} value, the difference $|\bar{n}^{LP11} - \bar{n}^{LP01}|$ would be also infinitesimal ($\bar{n}^{LP\mu\nu}$ is bounded by n_{co} and n_{cl}) as well as $|\bar{n}_g^{LP11} - \bar{n}_g^{LP01}|$ (proportional to DMD) since $\bar{n}_g^{LP\mu\nu} = \bar{n}^{LP\mu\nu} + \lambda \cdot [d\bar{n}^{LP\mu\nu}/d\lambda]$. Therefore, reduction of

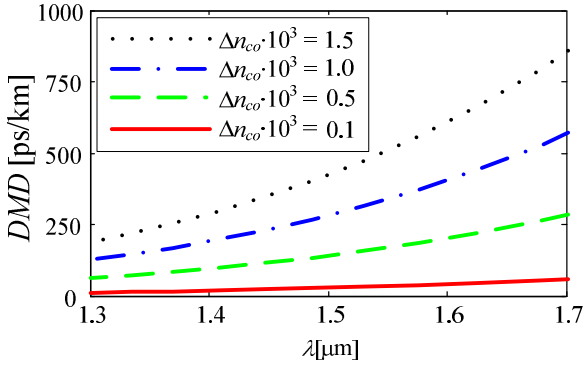

Fig. 2. *DMD* [ps/km] as a function of λ, for different Δn_{co} values.

Δn_{co} has the potential to further reduce the DMD values obtained in [19]. The drawback of the utilization of a low Δn_{co} is related to MBL. According to [20], the power loss at bends increases with decreasing Δn_{co} for a certain curvature radius and, as a consequence, low DMD and low MBL are opposite requirements. The trade-off between DMD and MBL on the optimization of Δn_{co} is analyzed in Section IV.

The MSI profile is shown in Fig. 1 (b), where each step *i* has an arbitrary Δn value (Δn_i) and step width w_{st}. The number of steps is N_{st}. The MSI profile allows evaluating arbitrary profiles by simultaneously increasing N_{st} and decreasing w_{st}.

III. Optimization Function and Algorithms

In this section, the optimization function used to search for the optimum parameters of each profile is presented, as well as the optimization algorithms for each profile. The optimization parameters of each profile can be gathered in a parameter vector (pv): $pv = [\alpha, \Delta n_{co}, \Delta n_{tr}, w_2, w_3]$ for the GCCT profile and $pv = [w_{st}, \Delta n_1, \ldots, \Delta n_{N_{st}}]$ for the MSI profile.

A. Optimization Function

The optimization function takes into account two figures: one related to DMD and another related to MBL. The DMD related figure is the maximum DMD among the guided modes and over the defined wavelength range (*maxDMD*), given by:

$$maxDMD(pv) = \max_{\lambda}\left(\max_{\mu\nu}\left|DMD_{LP\mu\nu}(\lambda, pv)\right|\right) \quad (3)$$

The MBL related figure is the curvature radius (R_c) for 100 turns and MBL = 0.1 dB at 1625 nm. For a given *x*M, the R_c of each mode is calculated and the highest value is considered. Considering the ITU-T recommendation in [24], R_c must be lower than or equal to 30 mm. The optimization function (*OF*) is given by:

$$OF(pv) = maxDMD(pv)\cdot\left\{1+\varepsilon\cdot\left[\beta\cdot\frac{(R_c-30)}{30}\right]\right\}$$
$$\beta = \begin{cases}0, & for\ R_c \le 30\\ 1, & for\ R_c > 30\end{cases} \quad (4)$$

with R_c in millimeter units.

where the ε factor can be 0 or 1 in order to consider or ignore the $R_c \le 30$ mm requirement. The $\beta\cdot(R_c - 30)/30$ factor in (4) introduces a penalizing factor for solutions with $R_c > 30$ mm, since β is equal to 0 for $R_c \le 30$ mm and equal to 1 for $R_c > 30$ mm. Note that, for each different *pv* tested, if the number of modes is not the desired the *OF* value is set to infinity. The optimization function (4) is subject to different sets of constraints depending on the profile being optimized. For the GCCT profile, *OF* is subject to the following constrains:

$$\left(\Delta n_{co}^{-} = 1\cdot10^{-3}\right) \le \Delta n_{co} \le \left(\Delta n_{co}^{+} = 5\cdot10^{-3}\right) \quad (5)$$
$$\left(\alpha^{-} = 1.5\right) \le \alpha \le \left(\alpha^{+} = 2.5\right) \quad (6)$$
$$\left(\Delta n_{tr}^{-} = -5\cdot10^{-3}\right) \le \Delta n_{tr} \le \left(\Delta n_{tr}^{+} = 0\right) \quad (7)$$
$$\left(w_2^{-} = 0\right) \le w_2 \le \left(w_2^{+} = w_1/2\right) \quad (8)$$
$$\left(w_3^{-} = 0\right) \le w_3 \le \left(w_3^{+} = w_1\right) \quad (9)$$
$$\left(\lambda^{-} = 1530\text{ nm}\right) \le \lambda \le \left(\lambda^{+} = 1565\text{ nm}\right) \quad (10)$$

Δn_{co}^{-} in (5) takes into account the difficulties of manufacturing Δn_{co} lower than $1\cdot10^{-3}$ [25] whereas Δn_{co}^{+} is used as upper bound of Δn_{co} taking into account that *maxDMD* increases with Δn_{co}. (6)-(9) were defined in [18]. (10) bounds λ to the C-band. In the MSI profile case, *OF* is subject to the following constrains:

$$\left(\Delta n_i^{-} = -5\cdot10^{-3}\right) \le \Delta n_i \le \left(\Delta n_i^{+} = 5\cdot10^{-3}\right) \quad (11)$$
$$N_{st} = \{16 \quad 32 \quad 64\} \quad (12)$$
$$\left(w_{st}^{-} = 0.5\ \mu\text{m}\right) \le w_{st} \le \left(w_{st}^{+} = 5\ \mu\text{m}\right) \quad (13)$$

(11) constrains the Δn_i of each step between $-5\cdot10^{-3}$ and $5\cdot10^{-3}$, taking into account the same reasoning used to set the constraints for Δn_{co} and Δn_{tr}. (12) constrains N_{st} to powers of 2 between 16 and 64, since a lower number of steps would not have sufficient flexibility to reduce *maxDMD* and R_c at the same time, and a higher N_{st} would be too complex to manufacture. (13) constrains w_{st} between 0.5 μm and 5 μm, such that the total length of the profile ($w_{st} \cdot N_{st}$) takes values similar to the total length considered for the GCCT profile ($w_1 + w_2 + w_3$). Moreover, λ is bounded to the C-band.

B. GCCT optimization algorithm

The optimization algorithm for the GCCT profile is designed to take advantage of the *maxDMD* function properties. In the order to present the *maxDMD* properties a 2M-FMF with $\Delta n_{co} = 1\cdot10^{-3}$, $w_2 = 3$ μm and $w_3 = 3$ μm is considered. Fig. 3 (a) presents the contour map of *maxDMD* as a function of (α, Δn_{tr}). Fig. 3 (a) shows that *maxDMD* is a convex function of (α, Δn_{tr}), such that $\min_{\alpha}(maxDMD)$ as a function of Δn_{tr} or $\min_{\Delta n_{tr}}(maxDMD)$ as a function of α, are convex functions. Fig. 3 (b) shows $\min_{\alpha}(maxDMD)$ as a function of Δn_{tr}. Therefore, the search for the pair (α, Δn_{tr})

that minimizes *maxDMD* for a given (Δn_{co}, w_2, w_3) point can be done one dimension at a time using for instance a golden section search (GSS) [26]. The GSS over α and the GSS over Δn_{tr} are arranged as:

$$maxDMD^{min}\left(\Delta n_{co}, w_2, w_3\right) = \min_{\alpha,\Delta n_{tr}}\left(maxDMD\left(pv\right)\right) = \text{GSS}\left(\Delta n_{tr}^{-}, \Delta n_{tr}^{+}, \text{GSS}\left(\alpha^{-}, \alpha^{+}, maxDMD\left(pv\right)\right)\right) \quad (14)$$

The first and second GSS function parameters are the lower and the upper bound, respectively, of the independent variable of the function under optimization. Further results have shown that considering different numbers of modes and (Δn_{co}, w_2, w_3) values within the domains defined in (5)-(10), the *maxDMD* function properties presented are still valid.

Finally, in order to find the full optimum *pv* set, an exhaustive search (ES) is performed over $maxDMD^{min}$(Δn_{co}, w_2, w_3). The GSS optimizes α and Δn_{tr} with a termination tolerance on *maxDMD* of 0.001 ps/km. The ES optimizes the Δn_{co}, w_2 and w_3 with tolerances of $5\cdot10^{-4}$, 0.25 μm and 0.5 μm, respectively. Further reducing these tolerances by a factor of 2 changed *maxDMD* negligibly.

C. MSI optimization algorithm

The optimization algorithm used for the MSI profile is a genetic algorithm (GA), due to the high number of optimization parameters. The individual genes are: [w_{st}, Δn_1, …, Δn_{Nst}], and the individual fitness is given by the inverse of *OF* in (4) considering $\varepsilon = 1$.

The initial population is randomly generated within the predefined Δn_i and w_{st} constraints given by (11) and (13), respectively. The Δn_i genes are generated using an uniform distribution and the w_{st} gene is generated using a Gaussian distribution with mean equal to $(w_1+w_2+w_3) / N_{st}$, considering the optimum GCCT parameters obtained with $\Delta n_{co} = 0.001$, and standard deviation equal to $(w_{st}^{+} - w_{st}^{-})/6$. The size of the initial population is 2000. After the first generation the population size is reduced to 200. The following generations are created using crossover, mutation and selection operators.

The crossover operator randomly selects the j^{th} gene in the solution structure and, given two parents $X = [w_{st}^{X}, \Delta n_1^{X}, \ldots, \Delta n_{Nst}^{X}]$ and $Y = [w_{st}^{Y}, \Delta n_1^{Y}, \ldots, \Delta n_{Nst}^{Y}]$, the generated offspring are constructed as: $U = [w_{st}^{X}, \Delta n_1^{X} \ldots, \Delta n_{j-1}^{X}, \Delta n_j^{Y}, \ldots, \Delta n_{Nst}^{Y}]$ and $W = [w_{st}^{Y}, \Delta n_1^{Y} \ldots, \Delta n_{j-1}^{Y}, \Delta n_j^{X}, \ldots, \Delta n_{Nst}^{X}]$. The selection of the individuals for the crossover operation is executed using a roulette wheel selection scheme. In this scheme, the probability of an individual being selected is proportional to its fitness. The size of the offspring generated is 200.

The mutation operation is executed adding to the l^{th} gene (randomly selected) a Gaussian random variable with zero mean and standard deviation σ_l. The standard deviation σ_l is weighed by the domain of the l^{th} gene, in order to compensate for the different orders of magnitude between w_{st} and Δn_i. σ_l is given by: $(w_{st}^{+} - w_{st}^{-})/6$ for $l = 1$ and $(\Delta n_i^{+} - \Delta n_i^{-})/6$ for $l > 1$. In each generation, the mutation operation is applied to the offspring with a probability of 50 %. Additionally, 20 new individuals are added to the offspring selecting the 20 best parents (parents with higher fitness) and applying the mutation operator (the original parents are kept in the population).

In the process of selection of the next generation, 10 % of the best individuals (individuals with higher fitness) are always chosen, and the remaining population is selected using the roulette wheel selection scheme already used in the crossover operation.

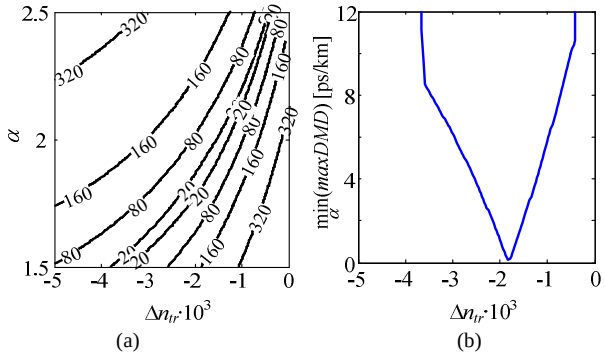

Fig. 3. (a) Contour map of *maxDMD* [ps/km] as a function α and Δn_{tr}. (b) $\min_{\alpha}\left(maxDMD\right)$ as a function of Δn_{tr}.

IV. Optimization Results

The optimization results are shown in this section for the GCCT and MSI profiles. The *maxDMD* and R_c are required to be equal or lower than 12 ps/km and 30 mm, respectively.

A. GCCT Profile

In this sub-section the optimum results for the GCCT profile are presented. Fig. 4 (a) and (b) show *maxDMD* and R_c optimum values, respectively, as a function of Δn_{co}, obtained using *OF* with $\varepsilon = 0$ and $\varepsilon = 1$.

Fig. 4 (a) shows that *maxDMD* decreases with decreasing Δn_{co} for all numbers of modes, in line with the explanation provided in Section II, independently of ε. Fig. 4 (b) shows that R_c increases when Δn_{co} decreases for $\varepsilon = 0$, such that for $\Delta n_{co} < 5\cdot10^{-3}$ the R_c requirement is not satisfied for all the numbers of modes considered. On the other hand, considering $\varepsilon = 1$, Fig. 4 (b) shows that the R_c requirement is satisfied for all Δn_{co} values and numbers of modes considered, $1\cdot10^{-3} \le \Delta n_{co} \le 5\cdot10^{-3}$. Comparing the results shown in Fig. 4 (a) obtained using $\varepsilon = 0$ and $\varepsilon = 1$, it can be concluded that the R_c requirement can be satisfied from 2M to 12M with small *maxDMD* degradation (lower than 0.5 ps/km for $\Delta n_{co} = 1\cdot10^{-3}$). Therefore, Fig. 4 shows that the *maxDMD* and R_c requirements are satisfied simultaneously for $1\cdot10^{-3} \le \Delta n_{co} \le 4\cdot10^{-3}$ from 2M to 12M. Moreover, it can be concluded that *maxDMD* cannot be reduced to negligible levels (*maxDMD* < 0.1 ps/km) for more than 2M. This limitation is explained noting that the field confinement effect of the trench affects each higher-order mode (LP02, LP21, LP12, LP31, …) with different strength, since all have a considerable power concentration near the core boundary but different distributions [19]. Therefore, each mode has a different optimum trench dimensioning and it is not possible to reduce the DMD of all modes to negligible values at the same time over the C-band. Moreover, increasing the number

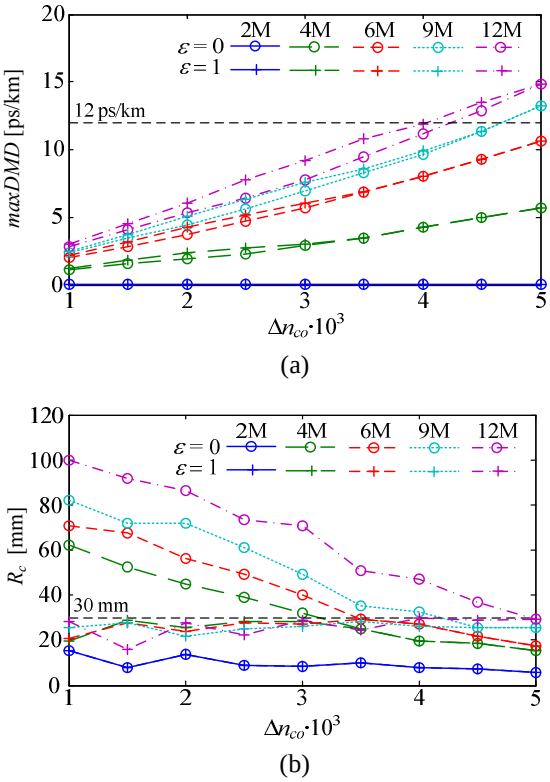

Fig. 4. (a) *maxDMD* [ps/km] optimum values as a function of Δn_{co} for different numbers of modes. (b) R_c [mm] as a function of Δn_{co} for different numbers of modes.

TABLE I
OPTIMIZED FIBER PARAMETERS AND CHARACTERISTICS FOR THE OPTIMUM GCCT PROFILE WITH $\Delta n_{co} = 0.001$ AND $\varepsilon = 1$

	Number of modes				
	2	4	6	9	12
α	2.15544	1.96677	1.97257	1.97291	1.97228
$\Delta n_{tr}\cdot 10^3$	-3.1221	-2.9888	-3.4030	-3.2370	-3.3598
w_1[μm]	19.2056	27.3020	33.8922	41.9886	48.7671
w_2[μm]	6	4.5	5.5	6	6.5
w_3 [μm]	2.5	1.5	1.5	1.5	1.5
maxDMD [ps/km]	0.004	1.347	2.252	2.487	2.997
R_c [mm]	15.1	19.9	20.8	25.6	28
min(D); max(D) [ps/(nm·km)]	22.4;22.5	22.4;22.5	22.4;22.5	22.4;22.5	22.3;22.6
min(S); max(S) [fs/(nm^2·km)]	65.5;65.6	63.0;65.7	61.9;65.8	61.3;65.8	57.3;65.9
γ- LP01 [W^{-1}/km]	0.222	0.161	0.130	0.105	0.09

of modes, the (α, Δn_{tr}, w_2, w_3) domain satisfying *maxDMD* ≤ 12 ps/km decreases for a given Δn_{co}.

The optimum parameters for $\Delta n_{co} = 1\cdot10^{-3}$ and $\varepsilon = 1$ are shown in Table I, as well as the respective *maxDMD*, R_c, chromatic dispersion (D) at 1550 nm (for the mode with highest D, max(D), and for the mode with lowest D, min(D)), chromatic dispersion slope (S) at 1550 nm (for the mode with highest S, max(S), and for the mode with lowest S, min(S)) and nonlinear coefficient (γ) for LP01 (the mode with the highest γ). Comparing with typical SSMF values, the D values are only slightly higher than ~17 ps/(nm·km), whereas the S values are lower than ~80 fs/(nm^2·km). The γ value is significantly lower than the SSMF typical value of 1.3 W^{-1}/km, as expected due to the higher core radius. In the Appendix, Table III provides for all modes the values of the: $DMD_{LP\mu\nu}$ for the worst wavelength of the C-band, D at 1550 nm, effective area (A_{eff}) at 1550 nm, and R_c.

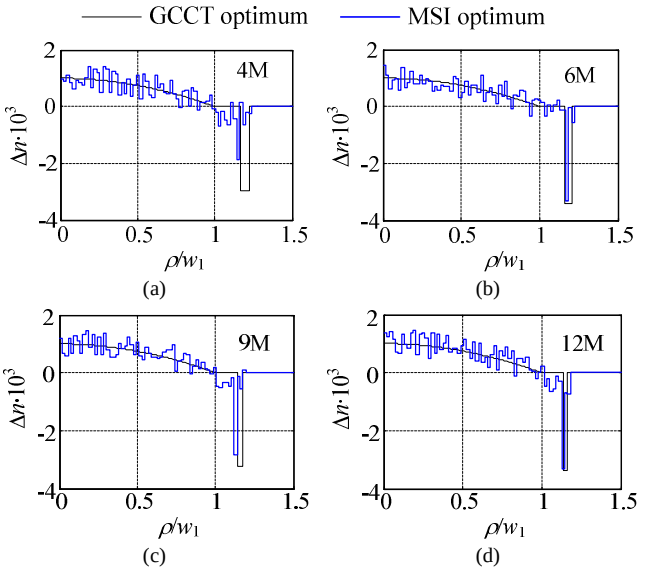

Fig. 5. Optimum MSI profile with 64 steps and optimum GCCT profile considering $\Delta n_{co} = 1\cdot10^{-3}$ as a function of ρ/w_1, for: (a) 4M, (b) 6M, (c) 9M and (d) 12M.

TABLE II
CHARACTERISTICS FOR THE OPTIMUM MSI PROFILES

N_{st}		Number of modes			
		4	6	9	12
16	*maxDMD* [ps/km]	1.21	3.10	3.51	5.26
	maxDMD red. [%]*	10.7	-36.8	-41.1	-75.6
	R_c [mm]	23.9	19.4	24.2	25
32	*maxDMD* [ps/km]	1.06	2.20	2.76	3.58
	maxDMD red. [%]*	21.3	3.1	-10.7	-19.5
	R_c [mm]	21.5	19.6	28.9	24.8
64	*maxDMD* [ps/km]	0.93	1.75	1.95	2.43
	maxDMD red. [%]*	31.3	22.9	21.8	19.1
	R_c [mm]	21.5	19.5	26.6	26.3

**maxDMD red.* [%] - is the relative difference between the *maxDMD* of the MSI profile and the *maxDMD* of the GCCT optimum profile with $\Delta n_{co} = 1\cdot10^{-3}$, for the same number of modes.

As a main conclusion, the results presented in this section allow stating that optimizing Δn_{co} allowed to fulfill the requirement of *maxDMD* ≤ 12 ps/km and R_c ≤30 mm, which was not achievable in [19].

B. MSI Profile

In this sub-section, the optimum results for the MSI profile obtained using the algorithm described in Section III-C are presented. The MSI profile is optimized for: 4M, 6M, 9M and 12M (2M is skipped since negligible *maxDMD* levels were obtained with the GCCT profile), considering N_{st} = [16, 32, 64].

Table II presents the *maxDMD* and R_c of the optimum MSI profiles at the end of 400 generations, for 160 different initial

populations. The results show that 64 steps are required to obtain a *maxDMD* value lower than the *maxDMD* of the optimum GCCT profile with $\Delta n_{co} = 1 \cdot 10^{-3}$, for 9M and 12M. Moreover, the *maxDMD* of the best individual decreases with N_{st}, for a given *x*M, due to the increase of the profile flexibility with N_{st}. For $N_{st} = 64$, the *maxDMD* reduction comparatively to the GCCT results ranges from 19 % to 31 %. Regarding the R_c values, the best individual meets the $R_c \leq 30$ mm constraint, for all the cases considered. Note that the individual fitness is given by the inverse of *OF* in (4) considering $\varepsilon = 1$. In the Appendix, Table III provides, for all modes, the values of the: $DMD_{LP\mu\nu}$ for the worst wavelength of the C-band, *D* at 1550 nm, effective area (A_{eff}) at 1550 nm, and R_c.

Fig. 5 shows the superposition of the optimum MSI profile with $N_{st} = 64$ and the optimum GCCT profile with $\Delta n_{co} = 1 \cdot 10^{-3}$, for 4M, 6M, 9M and 12M. Analyzing Fig. 5 it can be concluded that the optimum MSI profiles are similar to the optimum GCCT profile for $\Delta n_{co} = 1 \cdot 10^{-3}$. The similarity between profiles holds for smaller N_{st}.

In conclusion, the results presented in Table II show that the MSI profiles present lower *maxDMD* than the minimum achieved with a GCCT profile for all *x*M considered with $N_{st} = 64$. However, such *maxDMD* reduction is obtained at the expense of a more complex profile. In order to choose between these two types of profile, the tolerance to the manufacturing margins will be analyzed in Section V.

V. Manufacturing Margins

The optimized parameters in Section IV were obtained ignoring the finite precision margins of the manufacturing control processes. These margins lead to deviation of the manufactured fiber parameters from the optimum values, causing DMD deviations. Along this paper, the tolerance of the optimum profiles to parameters deviations is measured as the maximum tolerable deviation (MTD), positive or negative, such that *maxDMD* and R_c remains lower than 12 ps/km and 30 mm, respectively. The tolerance of each parameter is calculated considering the remaining parameters fixed at their optimum values, except for the layers widths. All layers that compose the optimum profiles (GCCT or MSI) are simultaneously and proportionally changed.

In order to assess the probability of having a manufactured FMF satisfying the *maxDMD* and R_c requirements, the MTD values have to be compared to the statistics of parameters deviations on conventional multimode fibers (MMF). According to [27], parameters deviations are well described by normal distributions with a given standard deviation (σ). Therefore, for a specific parameter, when the MTD value is close to σ, 2σ or 3σ, the manufacturing success probability is approximately 68 %, 95 % or 99.7 %, respectively.

In this paper, the σ values of the parameters are defined considering as reference the standard requirements and profile distortions reported for MMFs of category OM3. Note that the OM1 and OM2 categories are not considered because the profile distortions reported for these categories would lead to a very low probability of success in the design of FMFs [28]. The σ of Δn ($\sigma_{\Delta n}$) is $5 \cdot 10^{-5}$, according to [25], applicable to

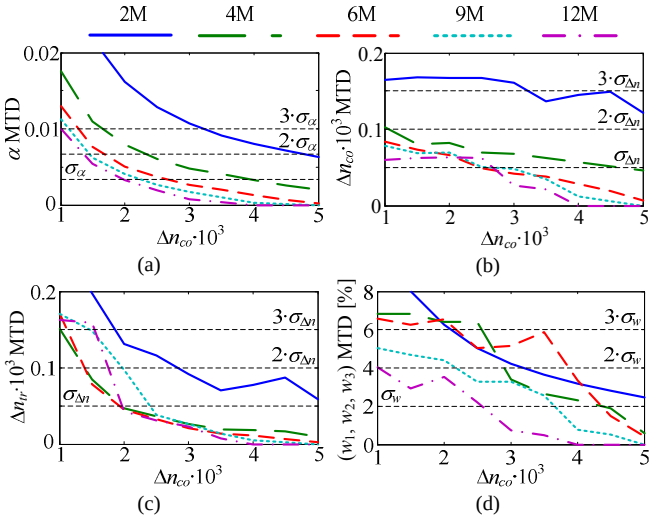

Fig. 6. GCCT profile parameters MTD: (a) α, (b) Δn_{co}, (c) Δn_{tr} and (d) (w_1, w_2, w_3).

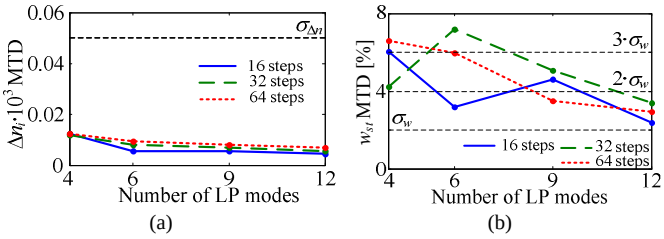

Fig. 7. MSI profile parameters MTD: (a) Δn_i and (b) w_{st}.

Δn_{co}, Δn_{tr} and Δn_i parameters. The σ of the layers widths (σ_w) is 2 % of the respective mean layer width (w_1, w_2, w_3, or w_{st}), taking into account that [25] states that the σ of the core radius of a conventional MMF (25 µm) is 0.5 µm. The σ of α (σ_α) is 0.003, taking into account the tolerance specified in [29].

A. GCCT Profile

In this sub-section the MTD of the GCCT profile parameters are presented, considering the optimum parameters values obtained in Section IV-A with $\varepsilon = 1$.

Fig. 6 (a), (b), (c) and (d) show the MTD of α, Δn_{co}, Δn_{tr}, and (w_1, w_2, w_3), respectively. It has been verified that the MTD is always limited by the *maxDMD* requirement. In most cases, two trends can be identified in Fig. 6, namely: the increase of the MTD with the decrease of Δn_{co} and the decrease of MTD with *x*M increase. Exceptions to these trends are a consequence of considering an optimization algorithm targeting the absolute minimum *maxDMD*, since further results have shown that non-optimum parameters can lead to a higher MTD. The MTD decrease with *x*M increase can be understood noting two different facts: in the absence of any deviation of the parameters, the absolute minimum *maxDMD* increases with *x*M for a given Δn_{co}, getting closer to 12 ps/km; it has been verified that *maxDMD* changes more abruptly around the optimum parameters with the increase of *x*M. Such facts are responsible for the (α, Δn_{tr}, w_2, w_3) domain reduction satisfying $maxDMD \leq 12$ ps/km with *x*M, as identified in

Section IV-A.

The MTD results in Fig. 6 allow estimating the probability of having a manufactured FMF with a *maxDMD* ≤ 12 ps/km and $R_c \leq 30$ mm for a given *x*M. For 2M, that probability is higher than 95 % for $\Delta n_{co} < 3 \cdot 10^{-3}$. Note that the success probability for $\Delta n_{co} = 4.5 \cdot 10^{-3}$ is closer to 68 %, limited by (w_1, w_2, w_3) MTD and Δn_{tr} MTD (as in [18]). In the case of 4M to 12M, the manufacturing probability goes from 95 % to 68 %, respectively, for $\Delta n_{co} = 1 \cdot 10^{-3}$, set by Δn_{co} MTD.

B. MSI Profile

In this sub-section, the MTD of the MSI profile parameters Δn_i and w_{st} are presented, considering the optimum parameters values obtained in Section IV-B. The Δn_i MTD of each step is calculated independently, but only the lowest Δn_i MTD is presented. Moreover, the Δn_i MTD for $N_{st} = 32$ and 64 is calculated considering pairs and quads of adjacent steps, since the w_{st} for $N_{st} = 16$ is used a reference. Fig. 7 (a) and (b) show the Δn_i MTD and w_{st} MTD, respectively, as functions of *x*M, considering N_{st} = [16, 32, 64]. As in the MTD analysis for the GCCT profile, it has been verified that the MTD is always limited by the *maxDMD* requirement.

Fig. 7 (a) shows that Δn_i MTD is 5 times lower than $\sigma_{\Delta n}$, with reduced dependency on N_{st} and on *x*M. Fig. 7 (b) shows that the w_{st} MTD is higher than σ_w for all N_{st} values, from 4M to 12M. These results, allow concluding that the probability of having a FMF with *maxDMD* ≤ 12 ps/km and $R_c \leq 30$ mm is approximately 16 %, set by the Δn_i MTD.

VI. Conclusions

In this work, the design of FMFs with low DMD over the C-band was investigated. Two different profiles have been considered: a GCCT profile and a MSI profile. The profiles parameters were optimized obtaining the lowest *maxDMD* achievable for 2M to 12M, with $R_c \leq 30$ mm. The optimization results have shown that the MSI profiles present lower *maxDMD* than the minimum achieved with a GCCT profile. Additionally, it has been concluded that *maxDMD* and R_c scale with *x*M. For 12M, it was obtained a *maxDMD* lower than 3 ps/km using a GCCT profile and lower than 2.5 ps/km using a MSI profile. Δn_{co} was shown to be the most preponderant parameter of the GCCT profile, allowing reducing *maxDMD* at the expense of increasing R_c. Regarding the optimum MSI profiles, it was shown that 64 steps are required to achieve a *maxDMD* improvement considering 12M. Furthermore, the impact of the fabrication margins on the optimum *maxDMD* was analyzed and used to derive the probability of having a manufactured FMF with *maxDMD* lower than 12 ps/km and R_c lower than 30 mm. For the GCCT profile it was shown that the probability increases with decreasing Δn_{co} whereas, the probability for the MSI profile has reduced dependency on N_{st} independently of *x*M. In the case of 12M, the probability was estimated to be approximately 68 % considering a GCCT profile and 16 % considering a MSI profile with 64 steps. In conclusion, the GCCT is the preferred profile with current fabrication margins.

Appendix

TABLE III
Characteristics for the optimum GCCT profile and optimum MSI profile

	Number of modes								
	2	4	4	6	6	9	9	12	12
	GCCT	GCCT	MSI	GCCT	MSI	GCCT	MSI	GCCT	MSI
	DMD* **[ps/km]**								
LP11	0.00	-1.35	0.91	-1.58	1.04	-1.14	-1.63	-1.21	1.06
LP02		-1.35	0.92	1.98	-1.70	-1.58	1.95	-1.27	1.18
LP21		-1.35	-0.93	-2.25	-1.74	-2.49	-1.72	-2.49	1.44
LP12				-1.58	0.77	-1.14	-1.88	-1.21	2.28
LP31				-2.25	1.75	-1.85	-1.93	-2.77	1.86
LP03						-2.40	1.65	2.81	2.43
LP22						-2.49	-0.98	-2.77	2.29
LP41						-1.85	1.86	-1.79	2.21
LP13								-2.49	-2.27
LP32								-1.79	-1.87
LP51								-3.00	-2.33
	***R*$_c$ [mm]**								
LP01	12.4	14.8	16.1	14.8	13.9	17.5	18.1	18.7	17.5
LP11	15.1	17.5	19.1	16.9	15.8	19.6	20.5	20.7	19.4
LP02		19.8	21.5	18.7	17.5	21.4	22.3	22.3	20.7
LP21		19.9	21.5	18.7	17.5	21.4	22.5	22.3	20.8
LP12				20.8	19.5	23.8	24.9	24.4	22.8
LP31				20.3	19.0	23.3	24.3	23.9	22.3
LP03						25.4	26.5	26.1	24.2
LP22						25.6	26.6	26.2	24.3
LP41						24.9	26.0	25.6	23.7
LP13								28.0	26.3
LP32								27.7	25.9
LP51								27.0	25.0
	***D* [ps/(nm·km)]**								
LP01	22.5	22.5	22.5	22.5	22.5	22.5	22.5	22.5	22.5
LP11	22.4	22.5	22.5	22.5	22.5	22.5	22.5	22.5	22.5
LP02		22.4	22.3	22.5	22.5	22.5	22.5	22.5	22.5
LP21		22.5	22.4	22.5	22.5	22.5	22.5	22.5	22.5
LP12				22.4	22.3	22.5	22.5	22.5	22.5
LP31				22.5	22.5	22.5	22.5	22.5	22.5
LP03						22.4	21.9	22.6	22.5
LP22						22.5	22.2	22.5	22.5
LP41						22.5	22.4	22.5	22.5
LP13								22.3	22.2
LP32								22.5	22.4
LP51								22.5	22.5
	***A*$_{eff}$ [μm^2]**								
LP01	476	645	653	813	727	1007	926	1167	1078
LP11	627	959	869	1096	1014	1355	1135	1571	1497
LP02		1390	1095	1680	1553	2077	1745	2393	2143
LP21		1250	1179	1462	1410	1805	1712	2094	1908
LP12				1724	1585	2213	2112	2561	2415
LP31				1731	1689	2166	2057	2508	2397
LP03						2928	2849	3593	3311
LP22						2667	2472	3202	2863
LP41						2454	2288	2870	2596
LP13								3307	3400
LP32								3616	3677
LP51								3145	3059

**DMD* of the worst wavelength of the C-band.

REFERENCES

[1] R. Essiambre, and R. Tkach, "Capacity Trends and Limits of Optical Communication Networks," *Proceedings of the IEEE*, vol. 100, no. 5, pp.1035-1055, May 2012.

[2] A. Ellis, J. Zhao, and D. Cotter, "Approaching the Non-Linear Shannon Limit," *J. Lightw. Technol*, vol. 28, no. 4, pp. 423-433, Feb. 15, 2010.

[3] R. Essiambre, and A. Mecozzi, "Capacity limits in single mode fiber and scaling for spatial multiplexing," in *Proc. OFC 2012*, pp. 1-3, paper OW3D.1

[4] P. Winzer, "Energy-Efficient Optical Transport Capacity Scaling Through Spatial Multiplexing," *IEEE Photon. Technol. Lett.*, vol. 23, no. 13, pp. 851-853, July1, 2011.

[5] B. Inan, *et al.*, "Equalizer complexity of mode division multiplexed coherent receivers," in *Proc. OFC 2012*, pp. 1–3, paper OW3D.4.

[6] A. Ellis, and N. Doran, "Are few-mode fibres a practical solution to the capacity crunch?," in *Proc. ICTON 2013*, pp. 1-4, paper Tu.C2.1.

[7] R. Ryf, N. Fontaine, and R. Essiambre, "Spot-Based Mode Couplers for Mode-Multiplexed Transmission in Few-Mode Fiber," *IEEE Photon. Technol. Lett.*, vol. 24, no. 21, pp. 1973-1976, Nov. 1, 2012.

[8] K. Sato, *et al.*, "Optimized graded index two-mode optical fiber with low DMD, large A_{eff} and low bending loss," *Opt. Express*, vol. 21, no. 14, pp. 16231-16238, 2013.

[9] L. Gruner-Nielsen, *et al.*, "Few mode transmission fiber with low DGD, low mode coupling and low loss," *J. Lightw. Technol.*, vol. 30, no. 23, pp. 3693-3698, Dec. 2012.

[10] N. Riesen, and J. Love, "Dispersion equalisation in few-mode fibres," *Opt. Quant. Electron.*, vol. 42, no. 9-10, pp. 577-585, Sept. 2011.

[11] E. Ip, *et al.*, "146λ×6×19-Gbaud wavelength- and mode-division multiplexed transmission over 10×50-km spans of few-mode fiber with a gain-equalized few-mode EDFA," in *Proc. OFC 2013*, pp. 1–3, paper PDP5A.2.

[12] M. Li, *et al.*, "Low delay and large effective area few-mode fibers for mode-division multiplexing," in *Proc. OECC 2012*, pp. 495–496, paper 5C3-2.

[13] R. Maruyama, *et al.*, "DMD Free Transmission Line Composed of TMFs with Large Effective Area for MIMO Processing," in *Proc. ECOC 2012*, pp. 1-3, paper Tu.1.F.2.

[14] R. Ryf, *et al.*, "12 x 12 MIMO Transmission over 130-km Few-Mode Fiber," in *Proc. FO 2012*, pp. 1-2, paper FW6C.4.

[15] T. Mori, *et al.*, "Low DMD Four LP Mode Transmission Fiber for Wide-band WDM-MIMO System," in *Proc. OFC 2013*, pp. 1-3, paper OTh3K.1.

[16] T. Sakamoto, T. Mori, T. Yamamoto, and S. Tomita, "Differential Mode Delay Managed Transmission Line for WDM-MIMO System Using Multi-Step Index Fiber," *J. Lightw. Technol.*, vol. 30, no. 17, pp. 2783-2787, Sept. 2012.

[17] R. Ryf, *et al.*, "32-bit/s/Hz Spectral Efficiency WDM Transmission over 177-km Few-Mode Fiber," in *Proc. OFC 2013*, pp. 1–3, paper PDP5A.1.

[18] F. Ferreira, D. Fonseca, and H. Silva, "Design of Few-Mode Fibers With Arbitrary and Flattened Differential Mode Delay," *IEEE Photon. Technol. Lett.*, vol.25, no.5, pp.438-441, Mar. 1, 2013.

[19] F. Ferreira, D. Fonseca, and H. Silva, "On the Dependence of Differential Mode Delay in Few-Mode Fibers on the Number of Modes," in *Proc. ICTON 2013*, pp. 1-4, paper Tu.C2.3.

[20] J. Sakai, and T. Kimura, "Bending loss of propagation modes in arbitrary-index profile optical fibers," *Appl. Opt.*, vol. 17, no. 10, pp. 1499–1506, 1978.

[21] C. Yeh, and G. Lindgren, "Computing the propagation characteristics of radially stratified fibers: an efficient method," *Appl. Opt.*, vol. 16, no. 2, pp. 483-493, 1977.

[22] W. Hermann, and D. U. Wiechert, "Refractive index of doped and undoped PCVD bulk silica," *Mater. Res. Bull.*, vol. 24, no. 9, pp. 1083–1097, 1989.

[23] M. Bigot-Astruc, D. Boivin, and P. Sillard, "Design and fabrication of weakly-coupled few-modes fibers," in *Proc. IEEE Photonics Society Summer Topical Meeting Series 2012*, paper TuC1.1.

[24] *Characteristics of a single-mode optical fibre cable*, Standard ITU-T G.652B, Oct. 2010.

[25] A. Bourdine, "Design of Refractive Index Profile for Multimode Optical Fibers with Low Differential Mode Delay," in *JOE*, vol. 1, pp. 1-9, April, 2013.

[26] W. Press, S. Teukolsky, W. Vetterling, and B. Flannery, *Numerical Recipes: The Art of Scientific Computing*, New York: Cambridge University Press, third edition, 2007.

[27] Krawarik P., Watkins L., "Fiber geometry specifications and its relations to measured fiber statistics", Applied Optics, 17(24), 3984-3989. 1978.

[28] A. Bourdine, D. Praporshchikov, and K. Yablochkin, "Investigation of defects of refractive index profile of silica graded-index multimode fibers," in Proc. of the SPIE, vol. 7992, no. 799206, pp. 1-6.

[29] P. Matthijsse, D. Molin, F. Gooijer, and G. Kuyt, "On the design of wide bandwidth window multimode fibers," in *Proc. IWCS 2005*, pp. 332–337.

(Please, do not include biographies if a new page is required.)

Filipe M. Ferreira was born in Coimbra, Portugal, in 1986. He received the B.S. and M.S. degrees in electrical and computer engineering from the University of Coimbra, Portugal, in 2008 and 2009, respectively. He is currently pursuing the Ph. D. degree in electrical and computer engineering at University of Coimbra.

In 2009, he joined the optical networks research group at Nokia Siemens Networks S. A. (now Coriant Portugal), Amadora, Portugal. His research interest includes optical transmission systems using mode division multiplexing, and design of few-mode fibers.

Daniel Fonseca was born in Lisbon, Portugal, in 1977. He joined the Siemens group in 2000 and has held several positions in research and development departments related to optical networking. In 2003, he joined the Research group of Nokia Siemens Networks S. A., Amadora, Portugal and received the Ph.D. degree in electrical engineering and computers from Instituto Superior Técnico (IST), Lisbon Technical University, Lisbon, Portugal, in 2008. His Ph. D. work focused on optical transmission systems using optical single sideband modulation format. Currently, he is the research manager for network optimization topics in Coriant Portugal (previous optical division from Nokia Siemens Networks) and his current research topics are multi-layer optimization and optical transmission design.

Henrique J. A. da Silva received the Ph. D. degree in communication systems engineering from the University of Wales, United Kingdom, in 1988. Since then he has been with the Department of Electrical and Computer Engineering at the University of Coimbra, where he is currently an associate professor and director of the Coimbra site of Instituto de Telecomunicações. His research interests include optical and mobile communication systems, with emphasis on photonic devices for telecommunications and optical transmission systems. He is a member of the Optical Society of America (OSA) and of the IEEE Communications and Photonics Societies.